

Nonuniform Sampling and Maximum Entropy Reconstruction in Multidimensional NMR

JEFFREY C. HOCH,^{†,*} MARK W. MACIEJEWSKI,[†] MEHDI MOBILI,[‡]
ADAM D. SCHUYLER,[†] AND ALAN S. STERN[§]

[†]University of Connecticut Health Center, Farmington, Connecticut 06030-3305, United States, [‡]Centre for Advanced Imaging, University of Queensland, St. Lucia, Queensland 4067, Australia, and [§]Rowland Institute at Harvard, Cambridge, Massachusetts 02142, United States

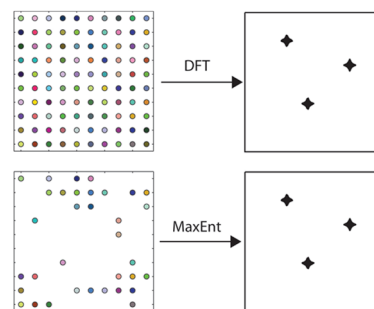
RECEIVED ON OCTOBER 17, 2013

CONSPECTUS

NMR spectroscopy is one of the most powerful and versatile analytic tools available to chemists. The discrete Fourier transform (DFT) played a seminal role in the development of modern NMR, including the multidimensional methods that are essential for characterizing complex biomolecules. However, it suffers from well-known limitations: chiefly the difficulty in obtaining high-resolution spectral estimates from short data records. Because the time required to perform an experiment is proportional to the number of data samples, this problem imposes a sampling burden for multidimensional NMR experiments. At high magnetic field, where spectral dispersion is greatest, the problem becomes particularly acute. Consequently multidimensional NMR experiments that rely on the DFT must either sacrifice resolution in order to be completed in reasonable time or use inordinate amounts of time to achieve the potential resolution afforded by high-field magnets.

Maximum entropy (MaxEnt) reconstruction is a non-Fourier method of spectrum analysis that can provide high-resolution spectral estimates from short data records. It can also be used with nonuniformly sampled data sets. Since resolution is substantially determined by the largest evolution time sampled, nonuniform sampling enables high resolution while avoiding the need to uniformly sample at large numbers of evolution times. The Nyquist sampling theorem does not apply to nonuniformly sampled data, and artifacts that occur with the use of nonuniform sampling can be viewed as frequency-aliased signals. Strategies for suppressing nonuniform sampling artifacts include the careful design of the sampling scheme and special methods for computing the spectrum. Researchers now routinely report that they can complete an N -dimensional NMR experiment 3^{N-1} times faster (a 3D experiment in one ninth of the time). As a result, high-resolution three- and four-dimensional experiments that were prohibitively time consuming are now practical. Conversely, tailored sampling in the indirect dimensions has led to improved sensitivity.

Further advances in nonuniform sampling strategies could enable further reductions in sampling requirements for high resolution NMR spectra, and the combination of these strategies with robust non-Fourier methods of spectrum analysis (such as MaxEnt) represent a profound change in the way researchers conduct multidimensional experiments. The potential benefits will enable more advanced applications of multidimensional NMR spectroscopy to study biological macromolecules, metabolomics, natural products, dynamic systems, and other areas where resolution, sensitivity, or experiment time are limiting. Just as the development of multidimensional NMR methods presaged multidimensional methods in other areas of spectroscopy, we anticipate that nonuniform sampling approaches will find applications in other forms of spectroscopy.



Introduction

NMR spectroscopy can probe all states of matter and quantify the composition of mixtures, structures of molecules, dynamics of rate processes, and thermodynamics of association. This versatility comes at a price; useful

sensitivity and high resolution require expensive magnets and lengthy experiments. The introduction of Fourier transform (FT) NMR enabled dramatic improvements in sensitivity and resolution.¹ In FT-NMR, the response of spins to a strong RF pulse is recorded, and the discrete FT (DFT) is used

to compute the spectrum. In 2D NMR, for example, a delay between two RF pulses, representing an “indirect” time dimension, is parametrically sampled by repeating the experiment using different values for the time delay. Successive Fourier transformation along the rows and the columns of the resulting data matrix yields a two-dimensional spectrum. FT-NMR readily generalizes to arbitrary numbers of dimensions,² enabling the resolution of individual nuclear resonances in complex systems.

The time required for a multidimensional NMR experiment is directly proportional to the number of samples in the indirect dimensions. Together, the requirements of uniform sampling (required by the DFT) with sufficiently small increments of the delay time to span the width of the spectrum (the Nyquist condition³) and long evolution times (for high resolution) mean that high-resolution spectra require lengthy experiments. Conversely, shorter experiments result in lower resolution spectra. Conventional uniform sampling in a high-resolution 3D experiment can require over a week of measuring time. While 3D experiments have become routine, resolution along the indirect dimensions is usually substantially less than the acquisition direct dimension. Four-dimensional experiments are far from routine because of the time required to collect data sufficient for even moderate resolution.

The subject of this Account is the use of nonuniform sampling (NUS) methods in multidimensional NMR. NUS permits high-resolution spectra to be obtained from short data records, drastically reducing experiment times. NUS can also be tailored to increase sensitivity. We focus on maximum entropy (MaxEnt) reconstruction, one of a number of non-Fourier methods of spectrum analysis suitable for NUS data, because it is particularly versatile and robust. Fast NMR methods are a burgeoning area of development,⁴ and NUS represents just one approach, but one of the most general.

The MaxEnt Method

MaxEnt reconstruction finds the spectrum that maximizes the entropy while maintaining consistency with the measured data. The use of entropy as a measure of missing information originated with Shannon and is the foundation for information theory.⁵ Consistency of the computed spectrum \mathbf{f} with the measured data \mathbf{d} is defined by the condition

$$C(\mathbf{f}, \mathbf{d}) = C_0 \quad (1)$$

where $C(\mathbf{f}, \mathbf{d})$ is the unweighted χ^2 statistic,

$$C(\mathbf{f}, \mathbf{d}) = \sum_{i=0}^{M-1} |m_i - d_i|^2 = \sum_{i=0}^{M-1} |\text{iDFT}(\mathbf{f})_i - d_i|^2 \quad (2)$$

and C_0 is an estimate of the noise level; iDFT is the inverse DFT, and \mathbf{m} is a “mock data” vector given by iDFT(\mathbf{f}). The constrained optimization problem is converted to an unconstrained optimization through introduction of a new objective function

$$Q(\mathbf{f}, \mathbf{d}) = S(\mathbf{f}) - \lambda C(\mathbf{f}, \mathbf{d}) \quad (3)$$

where $S(\mathbf{f})$ is the entropy. The unconstrained problem is to find the \mathbf{f} that minimizes $Q(\mathbf{f}, \mathbf{d})$, where the value of the Lagrange multiplier λ is adjusted to obtain $C = C_0$. $C(\mathbf{f}, \mathbf{d})$ and $S(\mathbf{f})$, and thus $Q(\mathbf{f}, \mathbf{d})$, readily generalize to multiple dimensions. The seminal development of the “Cambridge” algorithm,⁶ which is both robust and highly efficient, launched the modern application of the maximum entropy principle in NMR. Extensions to the Cambridge algorithm have provided additional performance gains and adapted it to the requirements of phase-sensitive NMR data.³

A schematic diagram for MaxEnt reconstruction is shown in Figure 1. Details of the algorithm have been given previously;³ however there are a number of features that are important for applications to NUS. At each iteration, \mathbf{m} is computed from the current value of \mathbf{f} . The computation of $C(\mathbf{f}, \mathbf{d})$ can be limited to arbitrary subsets of \mathbf{m} ; this is the basis for the application to nonuniform sampling methods. The value of λ is normally chosen so that $C(\mathbf{f}, \mathbf{d})$ converges to a value (C_0) that is comparable to the noise level in the data. For multidimensional spectra that are reconstructed by computing subspectra, for example, obtaining a 2D spectrum from a series of 1D spectra, using a fixed C_0 value can result in variations in λ that produce slight variations in the nonlinearity of the reconstruction. An alternative, called the fixed- λ algorithm,⁷ instead employs a fixed value of λ for all subspectra, with λ chosen so that the average value of $C(\mathbf{f}, \mathbf{d})$ over all subspectra is comparable to the noise. Another alternative is to constrain the reconstruction to match the empirical data very closely, that is, small C_0 (or large λ). In this approach, MaxEnt reconstruction becomes nearly linear.⁸ While the formal derivation of the MaxEnt algorithm specifies criteria for determining the value of C_0 and another parameter that appears in the complex entropy functional, applying those criteria in practice can be challenging. Fortunately the results of MaxEnt reconstruction are not terribly dependent on the precise values of the parameters over a wide range. A heuristic algorithm has been shown to automatically find useful values for the adjustable parameters.⁹

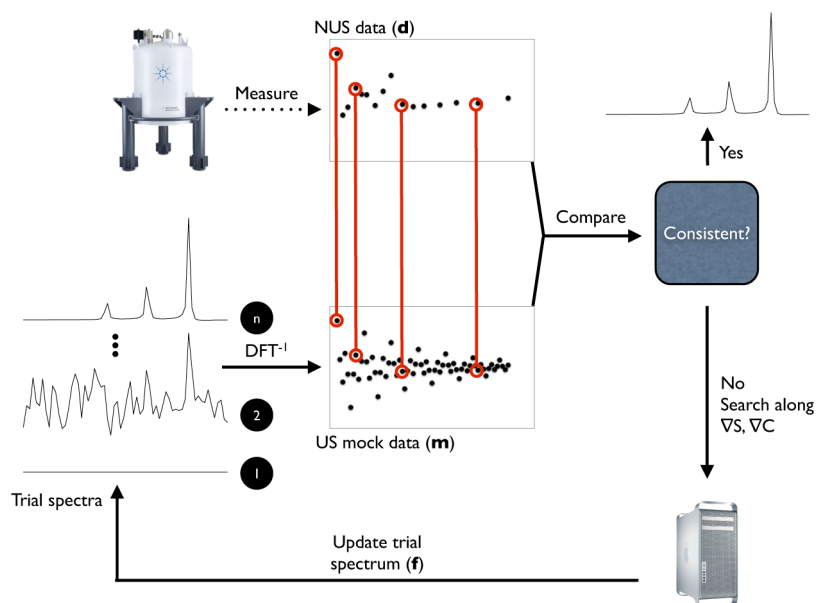


FIGURE 1. Schematic diagram for MaxEnt. MaxEnt reconstruction begins with empirical data and a preliminary trial spectrum \mathbf{f} (typically a blank spectrum). Spectrum \mathbf{f} is inverted (DFT^{-1}) to create “mock” data (\mathbf{m}) that is compared with the empirical data (\mathbf{d}). An update to the trial spectrum is computed by searching along the gradients of the entropy and the constraint (the agreement between the empirical and mock data). The algorithm converges to the unique MaxEnt solution when the gradient of the objective function $Q = S - \lambda C$ is zero and the gradients of S and C are antiparallel.

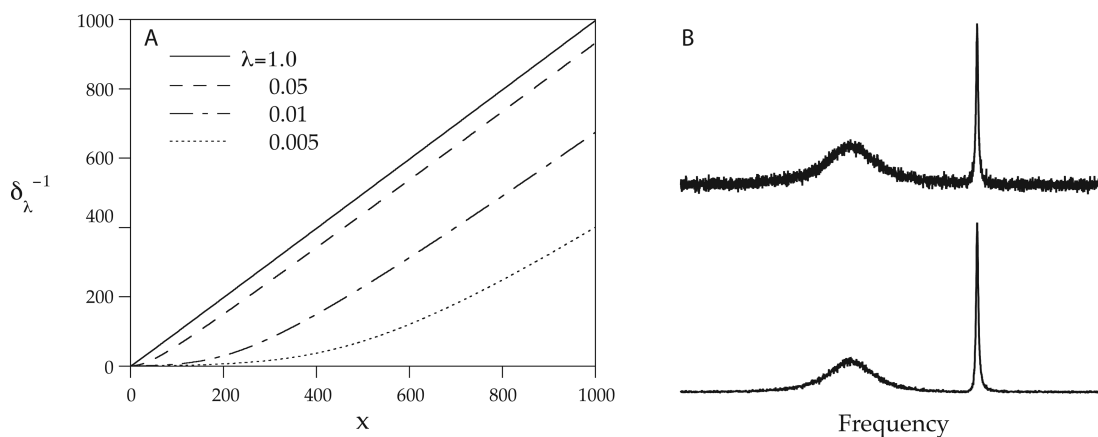


FIGURE 2. Nonlinear transformation for analytic MaxEnt. In the special case that MaxEnt is used to compute the n -element spectrum from an n -element FID, the MaxEnt spectrum is equivalent to applying a monotonic nonlinear transformation to the DFT of the FID. The nonlinear transformation (A) depends on the value of λ ; in the limit of large λ (the constraint weighted more heavily than the entropy), the transformation becomes nearly linear. For small λ , the transformation scales down small amplitude signals more than large amplitude signals (B).

While numerical solution is required in the general case, there is a special case where MaxEnt reconstruction has an analytical solution that gives insights into how MaxEnt reconstruction works. When N (the number of points in the reconstructed spectrum) is equal to M (the number of experimental data points), Parseval's theorem³ permits the constraint statistic to be computed in the frequency domain. The MaxEnt solution¹⁰ corresponds to a nonlinear transformation, applied point-by-point to the DFT of the time domain data. Figure 2 illustrates the transformation $\delta_{\lambda}^{-1}(x)$ for various values of λ (panel A). The transformation depends on

the value of λ and has the effect of scaling every point in the spectrum down, but points closer to the baseline are scaled down more than points far above the baseline (panel B). This explains why noise near the baseline is suppressed more effectively than noise superimposed on top of broad features. This result implies an important distinction between signal-to-noise ratio (SNR) and sensitivity. Applying the same transformation to both the signal and the noise cannot improve sensitivity, since peaks that are comparable in height to the noise level will be reduced by the same amount as the noise. The SNR may increase, but small peaks will be

just as difficult to distinguish as before. In this special case, gains in SNR in the MaxEnt reconstruction are purely cosmetic. In the more general case, there may be real sensitivity gains.^{11,12} However, a prudent investigator will always question whether gains in SNR really correspond to gains in sensitivity.¹⁰

The nonlinearity of MaxEnt has important implications when quantification of peak intensities or volumes is required, such as nuclear Overhauser effect measurements. One approach is to tightly constrain the reconstruction to match the data, which forces the reconstruction to be nearly linear (although at the expense of noise suppression).^{8,13} Another is to inject synthetic signals into the time domain data prior to reconstruction. A calibration curve can then be constructed by comparing measured intensities or volumes to the known amplitudes of the injected signals.¹⁴

MaxEnt is just one of a host of methods that have been developed as alternatives to the DFT for reconstructing spectra from NUS data. Some methods place restrictions on the way the data are sampled, for example along radial vectors in time. Others support arbitrary sampling schemes. Among the methods suitable for NUS data, MaxEnt is arguably the best characterized and most versatile. Strengths and weaknesses of the various methods have been compared recently.⁴

Sampling Fundamentals

The Nyquist sampling theorem states that to unambiguously determine frequencies, the sampling interval, Δt , must be at least as short as the reciprocal of the spectral width, SW spanned by frequency components in the signal. Frequencies higher than $1/\Delta t$ are aliased or mirrored about the spectral limits. The interval between frequency elements (the digital resolution) of the DFT is $1/(N\Delta t)$, where N is the number of samples collected; $N\Delta t$ is the maximum evolution time. The number of samples required to maintain a given maximum evolution time increases with magnetic field strength, because increasing field increases SW .

NUS schemes that sample a subset of the evolution times normally sampled using uniform sampling are called on-grid. In schemes such as radial, spiral, or concentric ring, the samples do not fall on this Cartesian grid.¹⁵ Exponentially biased random (on-grid) sampling was the first general NUS approach applied to multidimensional NMR.¹⁶ By analogy with matched filter apodization,¹⁷ biasing the sampling scheme toward shorter evolution times, using an exponential weighting to match the decay rate of the signal envelope, improves sensitivity. We refer to this as envelope-matched

sampling (EMS). Generalizations to sine-modulated signals, where the signal is small at the beginning, and constant-time experiments, where the signal envelope does not decay, utilize the same rationale.^{18,19} Distributions other than random have been employed; Poisson gap sampling²⁰ avoids long gaps between samples while ensuring that the samples are approximately randomly distributed.

It bears emphasizing that the Nyquist condition does not apply to NUS: NUS invariably introduces sampling artifacts that are a form of aliasing.²¹ To a good approximation, the positions and amplitudes of the sampling artifacts relative to true signals can be derived *a priori* from the sampling scheme. The point-spread function (PSF) is the spectrum of a real-valued sampling function \mathbf{K} consisting of the value 1 for samples included in the NUS scheme and the value zero for samples not included in the scheme. For on-grid sampling, the PSF can be computed using the DFT. \mathbf{K} has the property that when it multiplies a uniformly sampled data vector, element-wise, it results in a data vector in which the values not sampled in the NUS scheme have the value zero. The DFT of this zero-augmented NUS data (referred to as nonuniform DFT, nuDFT²²) is equal to the convolution of the DFT spectrum of the uniformly sampled data with the PSF. Thus, estimating the spectrum of an NUS data set is equivalent to deconvolving the PSF from the DFT spectrum of the zero-augmented data. While nuDFT provides useful insights into the nature of NUS artifacts, it is not a DFT of NUS data, nor is it a very good estimator of the spectrum of NUS data.

The PSF typically consists of a main central component at zero frequency surrounded by smaller nonzero frequency components. Because the PSF enters into the DFT of the zero-augmented data through convolution, each nonzero frequency component of the PSF gives rise to a sampling artifact for each signal component, with positions relative to the signal components that are the same as the relationship of the satellite peaks to the central component in the PSF. The amplitudes of the sampling artifacts are proportional to the amplitude of the signal component and the relative height of the satellite peaks in the PSF. Thus, the largest sampling artifacts arise from the largest-amplitude components of the signal spectrum. The useful dynamic range (ratio between the magnitude of the largest and smallest detectable signal components) of the DFT spectrum of the zero-augmented data can be directly estimated from the PSF as the ratio between the amplitudes of the zero-frequency component and largest nonzero frequency component; this ratio is the peak-to-sidelobe ratio (PSR). The ability of a method of spectrum analysis to suppress sampling artifacts

is ultimately limited by both the noise and the dynamic range of the signal.

In addition to the PSR, another useful metric for sampling schemes is the sensitivity relative to uniform sampling. The relative sensitivity depends on the sampling scheme and the nature of the signals, principally the decay rate (or R_2^*) of the signal envelope; in contrast the PSR depends only on the sampling scheme. The relative sensitivity, $r(\mathbf{K})$, of a sampling scheme with sampling function \mathbf{K} for a hypothetical signal can be estimated from the signal amplitude captured by a NUS scheme divided by that for uniform sampling having the same maximum evolution times, t_{\max} . For an exponentially decaying signal, the relative sensitivity of a scheme \mathbf{K} spanning a two-dimensional grid with size n_1 by n_2 is approximately given by²³

$$r(\mathbf{K}) = \frac{\sum_{i=1}^{n_1} \sum_{j=1}^{n_2} K_{ij} p_{ij}}{\sum_{i=1}^{n_1} \sum_{j=1}^{n_2} p_{ij}} \quad (4)$$

where the elements of \mathbf{p} are given by

$$p_{ij} = \exp \left\{ - \left(\frac{(i-1)R_2(1)}{SW(1)} \right) - \left(\frac{(j-1)R_2(2)}{SW(2)} \right) \right\} \quad (5)$$

$R_2(1)$ and $R_2(2)$ are the signal envelope decay rates, and $SW(1)$ and $SW(2)$ are the spectral widths in the two dimensions. A more accurate estimate would include the amount of noise captured by the NUS scheme compared with uniform sampling. Recently systematic efforts to improve sensitivity using NUS have been reported.^{8,24}

The magnitudes of artifacts in NUS spectra depend on the distribution of sampled evolution times and the sampling coverage $\gamma(\mathbf{K}) = k/N$, with k equal to the number of nonzero entries in \mathbf{K} and N the total number of elements in \mathbf{K} , which is the fraction of the evolution times from a uniform grid that are sampled by \mathbf{K} . For the example above, $\gamma(\mathbf{K}) = k/(n_1 \times n_2)$. In general, the PSR increases with increasing γ , with only the zero-frequency element of the PSF having a nonzero value for $\gamma = 1$. Because large values of the nonzero frequency components result from correlations among the sampled evolution times, \mathbf{K} composed of random evolution times will have the smallest sampling artifacts and highest PSR for a given coverage. For decaying sinusoids, a random sampling scheme will not have the highest sensitivity. A compromise between sensitivity and small artifacts leads to biased random sampling distributions, such as EMS.¹⁷ PSFs, together with PSRs and relative sensitivity, are shown in Figure 3

for some representative sampling schemes, for sampling coverages of 0.3, 0.1, and 0.05. The importance of randomness in sampling schemes for suppressing sampling artifacts has been explored in depth.^{21,25}

The resolution of any sampling scheme along a given dimension, whether uniform or nonuniform, is largely determined by t_{\max} . Using the DFT, resolving spectral features separated by the natural line width requires sampling at evolution times of πT_2 or longer, but sampling beyond $1.26T_2$ results in diminishing returns on sensitivity.²⁶ (Without apodization, SNR reaches its maximum at $1.26T_2$. Using matched filter apodization, SNR does not reach a maximum but reaches 96% of the limiting value at $1.26T_2$.) With MaxEnt, sampling to $1.26T_2$ usually resolves spectral components separated by the natural line width and thus represents a reasonable compromise between sensitivity and resolution for decaying signals. For experiments in which the evolution period is constant time, the signal decay is determined mainly by field inhomogeneity (RF and \mathbf{B}_0), and so practical limits on t_{\max} are imposed by the inhomogeneity or length of the constant time period, rather than T_2 .

The degree to which reducing sampling coverage via NUS can reduce experiment time, compared with uniform sampling, depends on a number of factors in addition to the randomness of the sampling scheme. Dynamic range of the signals and their amplitude relative to noise are key determinants. Because sampling artifacts enter through convolution, high dynamic range signals present challenges. Instead of being additive, the amplitudes of the largest sampling artifacts are determined by the amplitude of the strongest signal component. When the dynamic range is large, these artifacts may exceed the amplitude of weak signal components. Thus, more aggressive reductions in sampling coverage are feasible for high sensitivity experiments that have low dynamic range and are more challenging for experiments with low sensitivity or high dynamic range. Dimensionality and sparsity (the fraction of values with amplitudes close to zero) of the spectrum have also been shown to play a role.^{27,28} Increasing dimensionality helps in two ways, by decreasing the coherence of sampling and by increasing the sparsity of the spectrum. Sparsity helps because non-Fourier methods of spectrum analysis such as MaxEnt and l_1 -norm reconstruction work best for recovering sparse spectra.²⁸ As we show below, sampling coverage can conservatively be around 1/3 for each NUS dimension (e.g., roughly an order of magnitude reduction relative to uniform sampling for two indirect dimensions), even for challenging signals with high

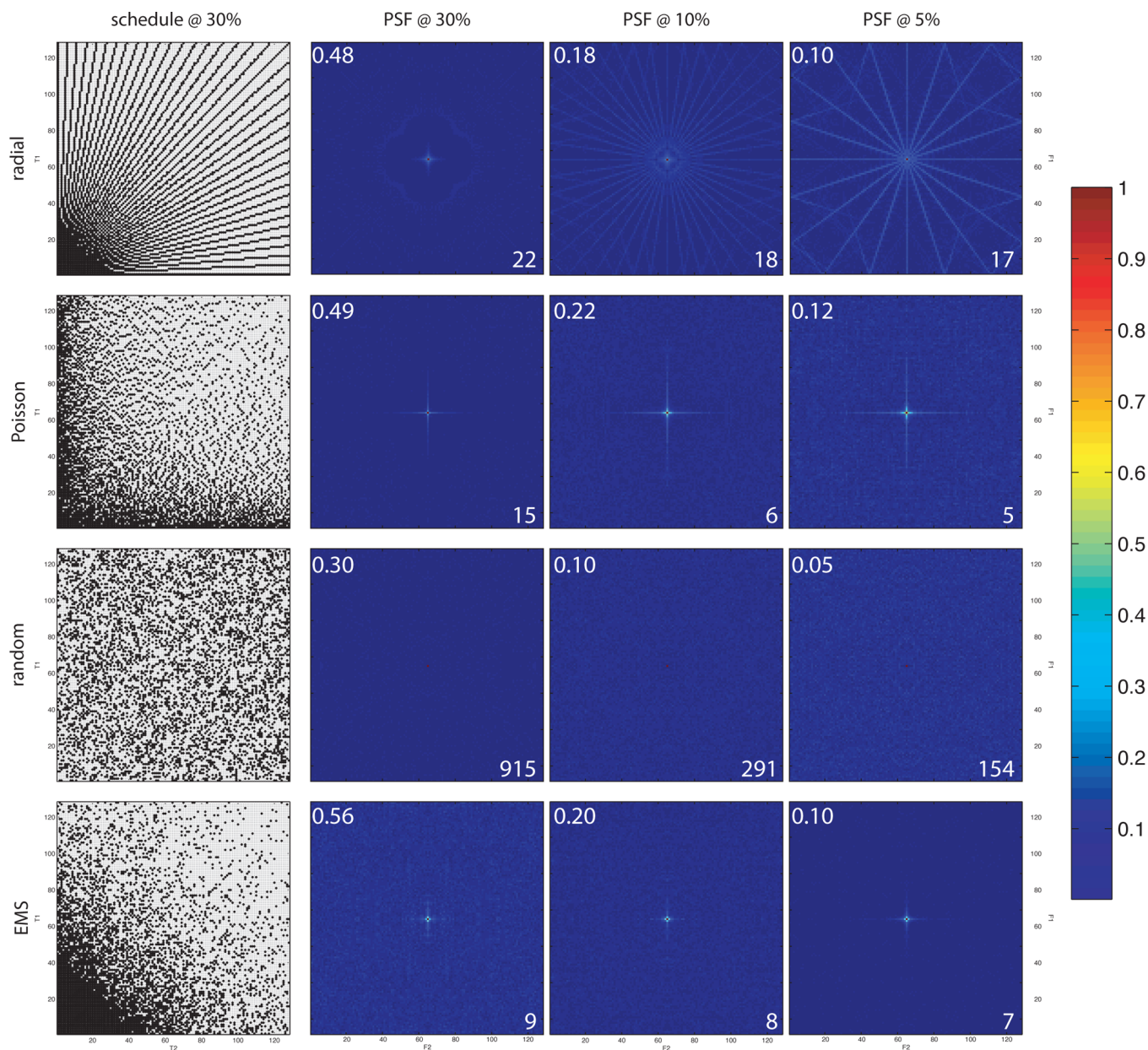


FIGURE 3. Examples of NUS schemes and PSFs. Examples of NUS sampling functions and PSFs in two nonuniformly sampled dimensions. Purely random sampling (third row) yields the smallest sampling artifacts for a given level of coverage (the central zero-frequency component is extremely narrow, making it hard to discern the red dot). Values for the relative sensitivity and PSR (both unitless) are displayed in the upper left and lower right, respectively, for each PSF.

dynamic range, while more aggressive reductions have been used successfully for low dynamic range signals.

Optimal Sampling. As noted above in the discussion of sensitivity, optimizing sampling schemes can be challenging. Additional optimization can be realized by adjusting the sampling grid. Nonuniform sampling on an oversampled grid has been shown to shift artifacts to the edges of the spectrum, outside the desired spectral window, although the magnitude of sampling artifacts is not affected.²⁹ Because a sampling scheme that is optimal for one signal will not

necessarily be optimal for a signal containing different frequency components, the design of efficient sampling schemes involves trade-offs. Simply put, no single NUS scheme will be best suited for all experiments. Despite these challenges, prior knowledge about the signal can successfully inform the design of efficient sampling schemes. One approach is to use “greedy” or adaptive sampling, in which a sampling scheme is iteratively generated by asking what sample (corresponding to a specific combination of indirect evolution times), added to samples already measured, will

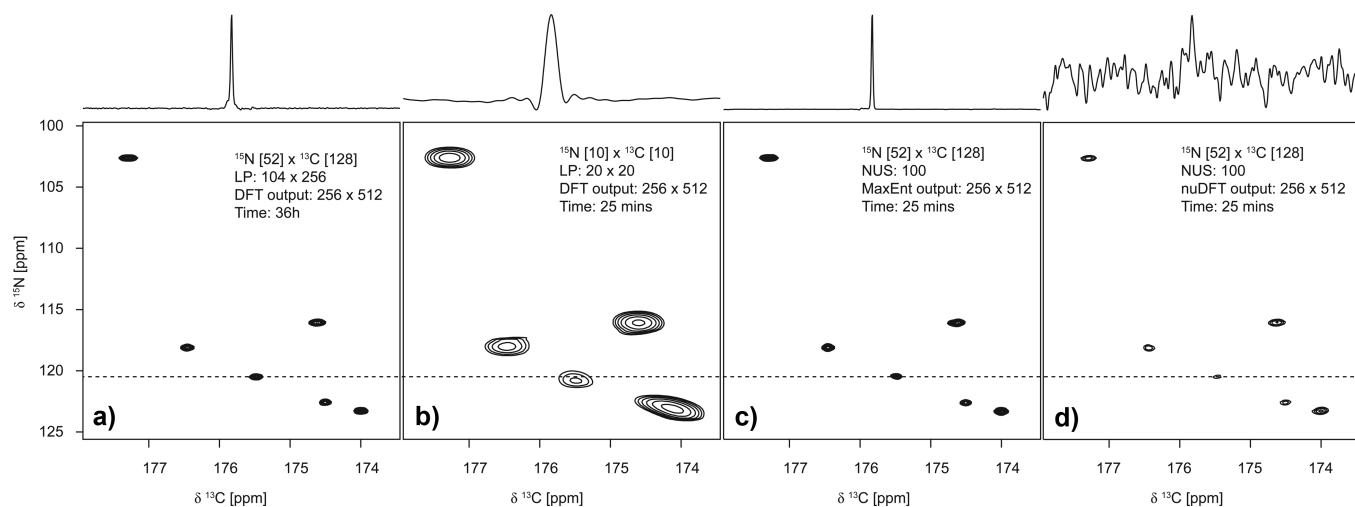


FIGURE 4. Three-dimensional HNCO spectra for ubiquitin at 14.1 T (600 MHz for ^1H). $^{13}\text{C}/^1\text{H}$ planar cross sections at a ^1H frequency of 8.14 ppm. The one-dimensional cross sections through the plots are of the ^{13}C row at the weakest peak (^{15}N frequency of 120.5 ppm), scaled so that the highest and lowest amplitudes are aligned. (A) Using a full data set, 6656 data samples, processed using LP extrapolation in each indirect dimension, shifted sine-bell apodization, and DFT; this data set required 36 h of data collection. (B) Using 100 uniformly sampled data points (10 increments in each indirect dimension); this data requires 25 min of data collection. The spectrum was computed by LP extrapolation in each indirect dimension, apodization using a shifted sine-bell, and DFT. (C) Using NUS, with 100 random samples selected according to an exponentially weighted distribution, reconstructed using MaxEnt; this data also requires 25 min of data collection. (D) Same as panel C, except using nuDFT instead of MaxEnt. The weak peak near the center of the ^{13}C trace in A is the “tail” of a peak at a nearby ^1H frequency; this disappears because of the narrower peaks in C.

most improve some metric of performance. Suitable metrics can be derived from the PSF (to minimize sampling artifacts), the relative sensitivity, the ability to resolve expected resonances based on statistical knowledge of chemical shift distributions,³⁰ or characteristics of the spectrum reconstruction prior to the next sample.^{31,32} A caveat is that while prior knowledge can greatly improve sampling efficiency when it is accurate, highly tailored sampling schemes can be less robust than more general sampling schemes when there are deviations from the underlying assumptions²³ or high levels of experiment noise.

NUS in Action

One compelling reason for adopting NUS in multidimensional NMR experiments is dramatic savings in data collection time without loss of resolution. The potential savings increase with magnetic field strength and with dimensionality. The time required for a multidimensional experiment is directly proportional to the number of evolution times sampled in the indirect dimensions,

$$t_{\text{exp}} = (t_{\text{acq}} + t_{\text{rc}})n_t k 2^{d-1} \quad (6)$$

where t_{acq} is the time required to sample one FID, t_{rc} is the recycle time between transients, n_t is the number of FIDs coaveraged, k is the number of samples in the indirect dimensions (for uniform sampling $k = \prod_{j=1}^{d-1} n_j$ with n_j the

number of samples in dimension j and the product being over the $d - 1$ indirect dimensions of a d -dimensional experiment), and the factor of 2 per indirect dimension reflects quadrature detection. For a fairly typical uniformly sampled 3D experiment averaging two FIDs with 64 evolution times sampled in each of two indirect time dimensions, a t_{acq} of 0.6 s and t_{rc} of 1.2 s, t_{exp} is 16.4 h. Contrast this time to an experiment in which the maximum evolution time in the indirect dimensions correspond to the Rovnyak limit²⁶ of $1.26T_2$ for optimizing sensitivity or πT_2 for resolving components separated by the natural line width. Typical ^{13}C and ^{15}N linewidths for a 20 kDa protein at 14.1 T (600 MHz for ^1H) are 17.5 and 5.8 Hz, respectively. The chemical shift dispersion for ^{13}C and ^{15}N is 10500 and 2100 Hz, respectively. With sampling intervals of 0.0952 and 0.476 ms required by the Nyquist condition, 241 samples in the ^{13}C dimension and 145 samples in the ^{15}N dimension would be required to sample uniformly to $1.26T_2$; 573 and 345 samples are needed to reach πT_2 . The value of t_{exp} for $1.26T_2$ is 140 h, and for πT_2 , it is 795 h. The total number of samples required for uniform sampling to either limit greatly exceeds the number typically acquired or the time devoted to data collection.³³ This means that higher dimensionality experiments that employ uniform sampling are

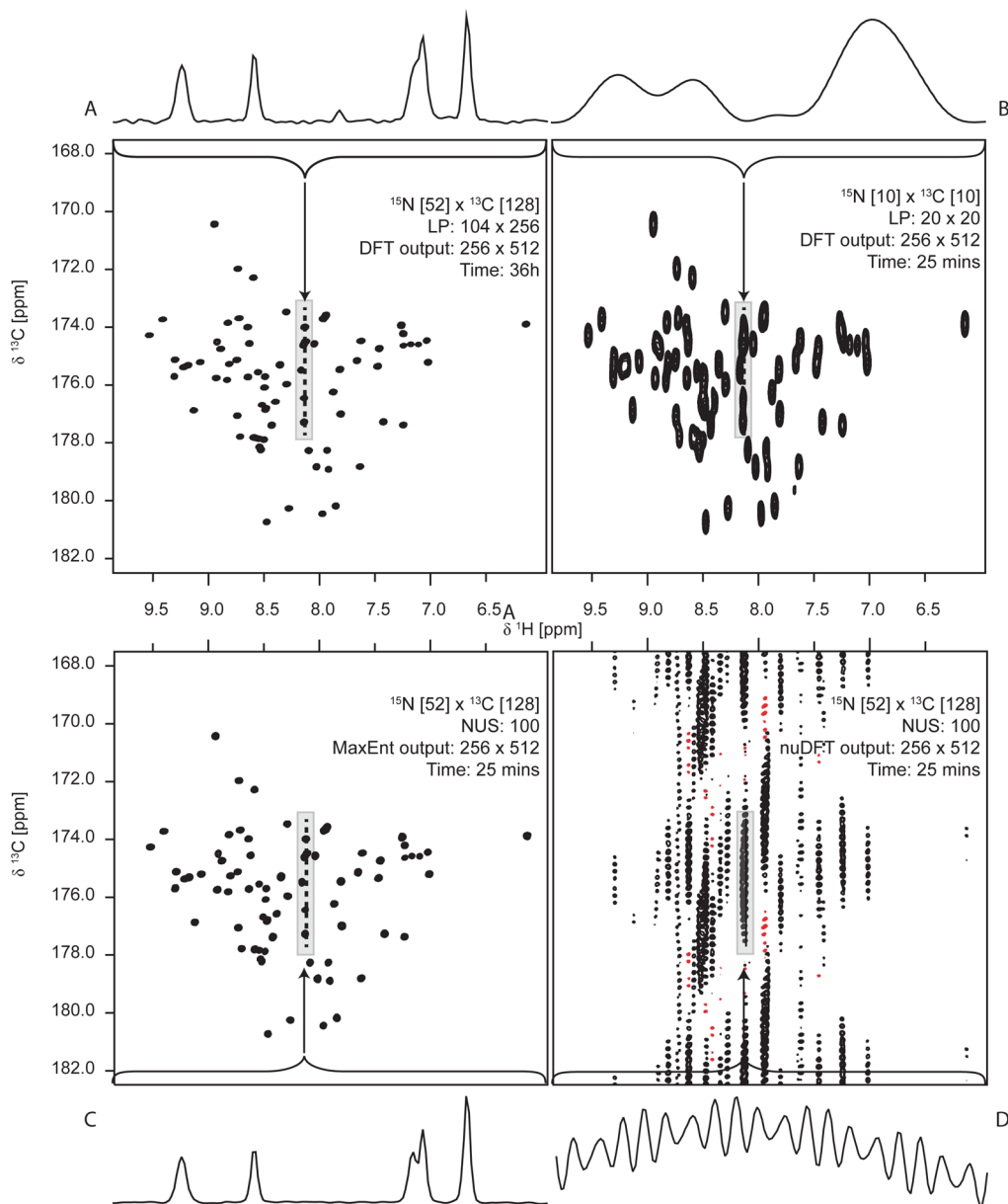


FIGURE 5. Three-dimensional HNCO spectra for ubiquitin at 14.1 T (600 MHz for ^1H). Projections of the full spectrum onto the $^{13}\text{C}/^1\text{H}$ plane. The one-dimensional cross sections through the plots are expansions depicted by the rectangular boxes, scaled to align the maxima and minima. (A) Using the full 6656 sample data set, processed using LP extrapolation in the indirect dimensions, shifted sine-bell apodization, and DFT (36 h of data collection); (B) using 400 uniformly sampled data points (20 increments in each indirect dimension, 25 min of data collection); the spectrum was computed by LP extrapolation in each indirect dimension, apodization using a shifted sine-bell, and DFT; (C) using NUS, with 400 random samples selected according to an exponentially weighted distribution, reconstructed using MaxEnt; this data also requires 25 min of data collection; (D) same as panel C, except using nuDFT instead of MaxEnt.

usually suboptimal both in sensitivity per unit time and in resolution.

In their seminal application of NUS and MaxEnt, Barna et al.³⁴ demonstrated rather conservative coverage ranging from 0.25 to 0.125. More substantial reductions in sampling coverage have subsequently been reported for 3D and 4D experiments, with coverages well below 0.01 common³⁵ and reaching 0.0016.³⁶ NUS is not the only means for

reducing the time required for multidimensional NMR experiments; in the SOFAST approach, the time between FIDs is reduced.³⁷ Because SOFAST (and related methods) and NUS are complementary, they can be combined, achieving greater speedup than either approach alone.^{29,38}

Rovnyak et al. exploited NUS to resolve separate resonances reflecting magnetically inequivalent ^{17}O nuclei in the unit cell of hydroxyapatite crystals.³⁹ NUS has also been

used to obtain high-resolution spectra for disordered proteins, which exhibit narrow spectral dispersion and hence crowded spectra.^{38,40,41} The higher resolution afforded by NUS has also enabled novel assignment strategies for protein spectra that are not practical with uniform sampling.^{35,42} For example, 4D HCC(CO)NH-TOCSY spectra obtained using NUS for the three indirect dimensions can be obtained in 1.5 days, a rather dramatic speedup, rendering high-resolution 4D experiments practical. The resulting resolution in the indirect dimensions is sufficient to capture unique carbon–proton connectivities, enabling a novel and efficient scheme for assigning protein side-chain resonances. Similar approaches have also been reported for backbone resonance assignment employing 3D experiments.^{42,43}

Examples illustrating important characteristics of NUS are shown in Figures 4 and 5. Figure 4 depicts 2D cross sections through the HNC0 spectrum of ubiquitin; 1D cross sections at the frequency indicated by the dashed line are shown above each contour plot. Panel A shows the spectrum obtained using conventional uniform sampling and DFT processing, requiring 34 h to complete the experiment. Panel B shows the results using uniform sampling with a truncated data set requiring 25 min to collect; the reduction in resolution is severe. Panels C and D show the results from an experiment also using 25 min of measuring time, but using NUS instead of uniform sampling. In Panel C, MaxEnt is used to compute the spectrum; in panel D, nuDFT was employed. Figure 5 depicts contour plots for 2D projections of the HNC0 spectrum for ubiquitin onto the ¹H–¹³C plane. Panel A shows the projection obtained using the uniformly sampled data set of Figure 4A. Panels B and C show the projections obtained from the truncated uniform and NUS data sets (corresponding to Figure 4, panels B and C, respectively). Panel D shows the projection obtained with nuDFT instead of MaxEnt (panel C); panel D dramatically reveals the poverty of nuDFT, because the coherent sampling artifacts are accumulated by the projection. The nearly 90-fold reduction in experiment time, with no loss of sensitivity or resolution, makes a convincing case for NUS and MaxEnt.

Concluding Remarks

The debate over optimal sampling schemes and the best reconstruction method is far from settled. A comprehensive critical comparison remains elusive, in part because metrics of spectral quality (sensitivity, resolution) that are valid for linear methods, such as DFT, are frequently not suitable for

non-Fourier methods. In addition to a lack of consensus on appropriate metrics, critical comparison is made difficult by the absence of a “shared task” comprised of a standard set of data. Nevertheless, a number of basic tenets of NUS have achieved broad consensus. It is abundantly clear that NUS approaches are essential for fully realizing the potential resolution afforded by modern high field magnets in the indirect dimensions of multidimensional experiments. Also widely appreciated is the importance of randomness in the design of sampling schemes in order to minimize sampling artifacts. Although the design of efficient sampling schemes remains an active area of investigation, it is understood that sampling more frequently when the signal envelope has greater amplitude improves sensitivity. The flexibility of NUS approaches for reducing measuring time, increasing resolution, or enhancing sensitivity, and in some cases two or more of these simultaneously, make NUS an indispensable tool for enhancing the utility and power of multidimensional NMR. These improvements will enable new and challenging applications of multidimensional NMR to larger, more complex, less abundant, and fleetingly stable systems.

We are grateful to many generous colleagues for inspiration and fruitful collaboration: Haribabu Arthanari, David Donoho, Dominique Frueh, Vitaliy Gorbatyuk, Sven Hyberts, Glenn King, Tatyana Polenova, David Rovnyak, Peter Schmieder, Jim Sun, and Gerhard Wagner. Support from the US National Institutes of Health (Grants RR-020125, GM-047467, and GM-102366) and the Australian Research Council (Grant FT110100925) is gratefully acknowledged.

BIOGRAPHICAL INFORMATION

Jeffrey Hoch is Professor of Molecular Biology and Biophysics and Director of the Gregory P. Mullen NMR Structural Biology Facility at the University of Connecticut Health Center. He obtained his Ph.D. from Harvard (1983) with Martin Karplus and Chris Dobson.

Mark Maciejewski is Assistant Professor of Molecular Biology and Biophysics and Manager of the Gregory P. Mullen NMR Structural Biology Facility at the University of Connecticut Health Center. For the past 20 years, he has utilized NMR for structural characterization of biomolecules and worked on NMR data processing.

Mehdi Mobli is an Australian Research Council Future Fellow at the Centre for Advanced Imaging at the University of Queensland, Australia. His research interests lie in developing and applying advanced NMR methods to solving difficult biological problems, including the structure and function of membrane proteins as well as characterizing weak intermolecular interactions.

Adam Schuyler is an Assistant Professor of Molecular Biology and Biophysics at the University of Connecticut Health Center. His

research interests include computational aspects of structural biology.

Alan Stern is a Staff Computational Scientist at Harvard's Rowland Institute. He has worked on NMR data processing for over 25 years.

FOOTNOTES

*Corresponding author. Mailing address: University of Connecticut Health Center, Dept. of Molecular Biology and Biophysics, 263 Farmington Ave., Farmington, CT 06030-3305 USA.

The authors declare no competing financial interest.

The manuscript was written through contributions of all authors. All authors have given approval to the final version of the manuscript.

REFERENCES

- Ernst, R. R.; Anderson, W. A. Application of Fourier transform spectroscopy to magnetic resonance. *Rev. Sci. Instrum.* **1966**, *37*, 93–102.
- Jeener, J. Oral Presentation, Ampere International Summer School, Basko Polje, Yugoslavia, 1971.
- Hoch, J. C.; Stern, A. S. *NMR Data Processing*, Wiley-Liss: New York, 1996.
- Mobli, M.; Hoch, J. C.; King, G. F. Fast Acquisition Methods in Multidimensional NMR. In *Advances in Biomedical Spectroscopy*, Dingley, A. J., Pascal, S. M., Eds.; IOS Press: Amsterdam, 2011.
- Shannon, C. E. A mathematical theory of communication. *Bell Syst. Tech. J.* **1948**, *27*, 379–423.
- Skilling, J.; Bryan, R. Maximum entropy image reconstruction: General algorithm. *Mon. Not. R. Astron. Soc.* **1984**, *211*, 111–124.
- Schmieder, P.; Stern, A. S.; Wagner, G.; Hoch, J. C. Quantification of maximum-entropy spectrum reconstructions. *J. Magn. Reson.* **1997**, *125*, 332–339.
- Paramasivam, S.; Suiter, C. L.; Hou, G.; Sun, S.; Palmer, M.; Hoch, J. C.; Rovnyak, D.; Polenova, T. Enhanced sensitivity by nonuniform sampling enables multidimensional MAS NMR spectroscopy of protein assemblies. *J. Phys. Chem. B* **2012**, *116*, 7416–7427.
- Mobli, M.; Maciejewski, M. W.; Gryk, M. R.; Hoch, J. C. An automated tool for maximum entropy reconstruction of biomolecular NMR spectra. *Nat. Methods* **2007**, *4*, 467–468.
- Donoho, D. L.; Johnstone, I. M.; Stern, A. S.; Hoch, J. C. Does the maximum entropy method improve sensitivity? *Proc. Natl. Acad. Sci. U. S. A.* **1990**, *87*, 5066–5068.
- Jones, J. A.; Hore, P. J. The maximum-entropy method - appearance and reality. *J. Magn. Reson.* **1991**, *92*, 363–376.
- Jones, J. A.; Hore, P. J. The maximum-entropy method and Fourier transformation compared. *J. Magn. Reson.* **1991**, *92*, 276–292.
- Hyberts, S. G.; Heffron, G. J.; Tarragona, N. G.; Solanky, K.; Edmonds, K. A.; Luithardt, H.; Fejzo, J.; Chorev, M.; Aktas, H.; Colson, K.; Falchuk, K. H.; Halperin, J. A.; Wagner, G. Ultrahigh-resolution (1)H-(13)C HSQC spectra of metabolite mixtures using nonlinear sampling and forward maximum entropy reconstruction. *J. Am. Chem. Soc.* **2007**, *129*, 5108–5116.
- Schmieder, P.; Stern, A. S.; Wagner, G.; Hoch, J. C. Quantification of maximum entropy reconstructions. *J. Magn. Reson.* **1997**, *125*, 332–339.
- Maciejewski, M. W.; Mobli, M.; Schuyler, A. D.; Stern, A. S.; Hoch, J. C. Data Sampling in Multidimensional NMR: Fundamentals and Strategies. In *Topics in Current Chemistry*, Billeter, M., Orekhov, V., Eds.; Springer: Berlin, 2012; pp 1–29.
- Barna, J. C. J.; Laue, E. D.; Mayger, M. R.; Skilling, J.; Worrall, S. J. P. Exponential sampling: an alternative method for sampling in two dimensional NMR experiments. *J. Magn. Reson.* **1987**, *73*, 69.
- Ernst, R. R. Sensitivity enhancement in magnetic resonance. *Adv. Magn. Reson.* **1966**, *2*, 1–135.
- Schmieder, P.; Stern, A. S.; Wagner, G.; Hoch, J. C. Application of nonlinear sampling schemes to COSY-type spectra. *J. Biomol. NMR* **1993**, *3*, 569–576.
- Schmieder, P.; Stern, A. S.; Wagner, G.; Hoch, J. C. Improved resolution in triple-resonance spectra by nonlinear sampling in the constant-time domain. *J. Biomol. NMR* **1994**, *4*, 483–490.
- Hyberts, S. G.; Takeuchi, K.; Wagner, G. Poisson-gap sampling and forward maximum entropy reconstruction for enhancing the resolution and sensitivity of protein NMR data. *J. Am. Chem. Soc.* **2010**, *132*, 2145–2147.
- Brethorst, G. L. Nonuniform sampling: Bandwidth and aliasing. *Concepts Magn. Reson.* **2008**, *32A*, 417–435.
- Kazmierczuk, K.; Kozminski, W.; Zhukov, I. Two-dimensional Fourier transform of arbitrarily sampled NMR data sets. *J. Magn. Reson.* **2006**, *179*, 323–328.
- Schuyler, A. D.; Maciejewski, M. W.; Arthanari, H.; Hoch, J. C. Knowledge-based nonuniform sampling in multidimensional NMR. *J. Biomol. NMR* **2011**, *50*, 247–262.
- Hyberts, S. G.; Robson, S. A.; Wagner, G. Exploring signal-to-noise ratio and sensitivity in non-uniformly sampled multi-dimensional NMR spectra. *J. Biomol. NMR* **2013**, *55*, 167–178.
- Hoch, J. C.; Maciejewski, M. W.; Filipovic, B. Randomization improves sparse sampling in multidimensional NMR. *J. Magn. Reson.* **2008**, *193*, 317–320.
- Rovnyak, D.; Hoch, J. C.; Stern, A. S.; Wagner, G. Resolution and sensitivity of high field nuclear magnetic resonance spectroscopy. *J. Biomol. NMR* **2004**, *30*, 1–10.
- Lustig, M.; Donoho, D.; Pauly, J. M. Sparse MRI: The application of compressed sensing for rapid MR imaging. *Magn. Reson. Med.* **2007**, *58*, 1182–1195.
- Donoho, D. L.; Johnstone, I. M.; Stern, A. S.; Hoch, J. C. Maximum entropy and the nearly black object (with discussion). *J. R. Stat. Soc.: Ser. B* **1992**, *54*, 41–81.
- Maciejewski, M. W.; Qui, H. Z.; Rujan, I.; Mobli, M.; Hoch, J. C. Nonuniform sampling and spectral aliasing. *J. Magn. Reson.* **2009**, *199*, 88–93.
- Eghbalnia, H. R.; Bahrami, A.; Tonelli, M.; Hallenga, K.; Markley, J. L. High-resolution iterative frequency identification for NMR as a general strategy for multidimensional data collection. *J. Am. Chem. Soc.* **2005**, *127*, 12528–12536.
- Wong, L. E.; Masse, J. E.; Jaravine, V.; Orekhov, V.; Pervushin, K. Automatic assignment of protein backbone resonances by direct spectrum inspection in targeted acquisition of NMR data. *J. Biomol. NMR* **2008**, *42*, 77–86.
- Cornilescu, G.; Bahrami, A.; Tonelli, M.; Markley, J. L.; Eghbalnia, H. R. HIF-C: A robust and fast method for determining NMR couplings from adaptive 3D to 2D projections. *J. Biomol. NMR* **2007**, *38*, 341–351.
- Hyberts, S. G.; Arthanari, H.; Wagner, G. Applications of non-uniform sampling and processing. *Top. Curr. Chem.* **2012**, *316*, 125–148.
- Barna, J. C. J.; Laue, E. D.; Mayger, M. R.; Skilling, J.; Worrall, S. J. P. Exponential sampling, an alternative method for sampling in two-dimensional NMR experiments. *J. Magn. Reson.* **1987**, *73*, 69–77.
- Mobli, M.; Stern, A. S.; Bermel, W.; King, G. F.; Hoch, J. C. A non-uniformly sampled 4D HCC(CO)NH-TOCY experiment processed using maximum entropy for rapid protein sidechain assignment. *J. Magn. Reson.* **2010**, *204*, 160–164.
- Stanek, J.; Augustyniak, R.; Koźmiński, W. Suppression of sampling artefacts in high-resolution four-dimensional NMR spectra using signal separation algorithm. *J. Magn. Reson.* **2012**, *214*, 91–102.
- Schanda, P.; Kupce, E.; Brutscher, B. SOFAST-HMQC experiments for recording two-dimensional heteronuclear correlation spectra of proteins within a few seconds. *J. Biomol. NMR* **2005**, *33*, 199–211.
- Marion, D. Combining methods for speeding up multi-dimensional acquisition. Sparse sampling and fast pulsing methods for unfolded proteins. *J. Magn. Reson.* **2010**, *206*, 81–87.
- Rovnyak, D.; Filip, C.; Itin, B.; Stern, A. S.; Wagner, G.; Griffin, R. G.; Hoch, J. C. Multiple-quantum magic-angle spinning spectroscopy using nonlinear sampling. *J. Magn. Reson.* **2003**, *161*, 43–55.
- Pannetier, N.; Houben, K.; Blanchard, L.; Marion, D. Optimized 3D-NMR sampling for resonance assignment of partially unfolded proteins. *J. Magn. Reson.* **2007**, *186*, 142–149.
- Moťáčková, V.; Nováček, J.; Zawadzka-Kazmierczuk, A.; Kazmierczuk, K.; Zidek, L.; Sanderová, H.; Krásný, L.; Koźmiński, W.; Sklenář, V. Strategy for complete NMR assignment of disordered proteins with highly repetitive sequences based on resolution-enhanced 5D experiments. *J. Biomol. NMR* **2010**, *48*, 169–177.
- Sun, Z. Y.; Frueh, D. P.; Selenko, P.; Hoch, J. C.; Wagner, G. Fast assignment of 15N-HSQC peaks using high-resolution 3D HNCcαNH experiments with non-uniform sampling. *J. Biomol. NMR* **2005**, *33*, 43–50.
- Frueh, D. P.; Sun, Z. Y.; Vosburg, D. A.; Walsh, C. T.; Hoch, J. C.; Wagner, G. Non-uniformly sampled double-TRÖSY hNcaNH experiments for NMR sequential assignments of large proteins. *J. Am. Chem. Soc.* **2006**, *128*, 5757–5763.